

Effect of consolidation parameters on mechanical properties of Cu-based bulk amorphous alloy consolidated by hot pressing

CAI An-hui¹, XIONG Xiang², LIU Yong², AN Wei-ke¹, ZHOU Guo-jun¹, LUO Yun¹, LI Tie-lin¹, LI Xiao-song¹

1. College of Mechanical Engineering, Hunan Institute of Science and Technology, Yueyang 414006, China;

2. State Key Laboratory of Powder Metallurgy, Central South University, Changsha 410083, China

Received 7 August 2011; accepted 5 April 2012

Abstract: $\text{Cu}_{50}\text{Zr}_{40}\text{Ti}_{10}$ bulk amorphous alloys were fabricated by hot pressing gas-atomized $\text{Cu}_{50}\text{Zr}_{40}\text{Ti}_{10}$ amorphous powder under different consolidation conditions without vacuum and inert gas protection. The consolidation conditions of the $\text{Cu}_{50}\text{Zr}_{40}\text{Ti}_{10}$ amorphous powder were investigated based on an $L_9(3^4)$ orthogonal design. The compression strength and strain limit of the $\text{Cu}_{50}\text{Zr}_{40}\text{Ti}_{10}$ bulk amorphous alloys can reach up to 1090.4 MPa and 11.9 %, respectively. The consolidation pressure significantly influences the strain limit and compression strength of the compact. But the mechanical properties are not significantly influenced by the consolidation temperature. In addition, the preforming pressure significantly influences not the compression strength but the strain limit. The optimum consolidation condition for the $\text{Cu}_{50}\text{Zr}_{40}\text{Ti}_{10}$ amorphous powder is first precompacted under the pressure of 150 MPa, and then consolidated under the pressure of 450 MPa and the temperature of 380 °C.

Key words: hot pressing; Cu-based amorphous alloy; strain limit; consolidation; mechanical property

1 Introduction

Bulk amorphous alloys have attracted considerable attention both in fundamental research and engineering application due to their many unique properties, such as excellent corrosion resistance, remarkably high strength and hardness, and large elastic deformation limit [1,2]. Most of bulk amorphous alloys are fabricated by casting methods, and their shape and size are seriously limited in the case of the alloys having relatively low glass forming ability, which also limits the range of their applications [3,4]. Powder metallurgy method can produce good amorphous microstructures, and has an advantage of fabricating larger bulk amorphous alloy products in variety of shapes than casting methods [5].

The powder metallurgy methods for consolidating amorphous alloy powders include hot/cold pressing [6–9], extrusion [10,11], rolling [12], spark plasma sintering [13–16], pulsed current sintering [17], microwave induced sintering [18], and so on. However, these consolidation methods require a vacuum condition, resulting in the limit of their engineering applications.

Some investigations on the powder consolidation have been conducted without vacuum protection. KIM et al [8] investigated the magnetic properties of Fe–Si–B amorphous powder cores prepared by cold pressing using phenol resin as a binder under the pressure of 18 t/cm². Although the glassy powder cores exhibited stable permeability in the high frequency of 10 MHz, their mechanical properties were undoubtedly worse due to the addition of the binder. ANDO et al [19] consolidated Nd–Fe–B amorphous powders using explosive compaction. Although the highly dense compact (>95% relative density) without cracks was obtained under an optimum condition, a very thin melted layer was observed at the interface of powder particles. DROZDZ et al [20] produced a bulk amorphous cast iron by powder compaction at a high pressure (7.7 GPa), and found that the samples pressed at room temperature exhibit big, well seen porosity. KIM et al [21] investigated the microstructure and mechanical properties of powder injection molded product of Cu-based amorphous powder, and found that the specimens sintered at 470 °C between T_g and T_x showed powders just stuck together, and the injection molded

Foundation item: Project (50874045) supported by the National Natural Science Foundation of China; Projects (200902472, 20080431021) supported by the China Postdoctoral Science Foundation; Project (10A044) supported by the Research Foundation of Education Bureau of Hunan Province of China

Corresponding author: CAI An-hui; Tel: +86-730-8648848; E-mail: cah1970@sohu.com
DOI: 10.1016/S1003-6326(11)61425-8

Cu-based amorphous powders were hardly sintered even at temperatures just below the melting temperature as most of amorphous phases were replaced by crystalline phases. These attempts indicate that it is difficult for obtaining ideal compacts that consolidated the amorphous powder without high temperature between T_g and T_x . Among all mentioned consolidation methods, hot pressing is simple in the equipment and technology. Therefore, how to obtain ideal bulk amorphous alloys using hot pressing between T_g and T_x without vacuum protection and degassing procedure is a challenge for speeding up engineering application of bulk amorphous alloys.

On the other hand, the main factors influencing the consolidation effect are the pressure, time, and temperature, respectively. KIM et al [13] investigated the effects of consolidation temperature (between T_g and T_x) and pressure (80 MPa and 300 MPa) on microstructures and mechanical properties of Cu-based bulk amorphous alloys consolidated by spark plasma sintering. They found that the density and compression strength increased with increasing the temperature at the pressure of 80 MPa and with the same consolidation time. The density and compression strength increased with increasing the consolidation time at the pressure of 80 MPa and at the same temperature. In addition, the compression strength increased with increasing the consolidation time at the pressure of 300 MPa and at the same temperature, inverse for the hardness. DROZDZ et al [20] investigated the consolidation behavior of as-milled Fe-based amorphous powder at high pressure (7.7 GPa) and at the elevated temperature below T_x using hot pressing. They found that the density increased with increasing the temperature, and the compaction processed at temperature up to 520 °C (approximately at T_x) enabled the production of bulk amorphous alloys. However, the significance of these factors on the properties of bulk amorphous alloys has scarcely been investigated. Thus it is important for further investigating the effect of these factors on the properties of bulk amorphous alloys fabricated by powder metallurgy without vacuum protection and degassing procedure.

It is well known that Cu–Zr–Ti alloy system is a good glass former whose critical dimension forming amorphous state can reach up to 5 mm [22]. The high ΔT_x (66.7 K [23]) of $\text{Cu}_{50}\text{Zr}_{40}\text{Ti}_{10}$ amorphous alloy indicates its high thermal stability, which is possible for investigating the effect of the consolidation temperature on its property. In addition, the hardness of $\text{Cu}_{50}\text{Zr}_{40}\text{Ti}_{10}$ alloy was the lowest in $\text{Cu}_{(50+x)}\text{Zr}_{(40-x)}\text{Ti}_{10}$ alloy system [24], which would be a good condition for the hot pressing.

In the present work, $\text{Cu}_{50}\text{Zr}_{40}\text{Ti}_{10}$ bulk amorphous alloys were obtained by the consolidation of

gas-atomized amorphous alloy powder by using hot pressing technique based on an $L_9(3^4)$ orthogonal test. Its strain limit and compression strength were investigated.

2 Experimental

2.1 Experimental plan

For the elaboration of experimental plan, the orthogonal method for three factors at three levels was adopted. The studied factors and the assignment of the corresponding levels are listed in Table 1. The chosen array is the $L_9(3^4)$ which has nine rows corresponding to the number of tests (8 degrees of freedom) with three columns at three levels, as listed in Table 2. The factors are assigned to the columns. The plan of experiments is made of nine tests (array rows), in which the first column is assigned to the preforming pressure (A), the second column to the consolidation pressure (B), the third column to the consolidation temperature (C), and the fourth column to the error (D), respectively.

Table 1 Assignment of levels to factors

Level	Preforming pressure (A)/MPa	Consolidation pressure (B)/MPa	Consolidation temperature (C)/°C
1	75	300	360
2	150	450	380
3	225	600	400

Table 2 Orthogonal array $L_9(3^4)$, compression strength σ_c , and strain limit of bulk amorphous alloys

Test No.	A	B	C	D	σ_c /MPa	Strain limit/%
1	1	1	1	1	600.2	5.6
2	1	2	2	2	1090.4	7.8
3	1	3	3	3	779.7	8.0
4	2	2	1	3	898.4	11.9
5	2	3	2	1	1043.0	10.7
6	2	1	3	2	799.9	7.4
7	3	3	1	2	1002.0	8.4
8	3	1	2	3	677.8	8.1
9	3	2	3	1	958.2	10.1

2.2 Experimental procedures

Master ingots of the $\text{Cu}_{50}\text{Zr}_{40}\text{Ti}_{10}$ alloy (composition is given in nominal mole fraction) were prepared by arc melting a mixture of high purity Cu, Zr and Ti in a Ti-gettered argon atmosphere. The glassy alloy powders were produced by a high pressure argon gas atomization method. Atomization of the $\text{Cu}_{50}\text{Zr}_{40}\text{Ti}_{10}$ alloy was carried out in a close coupled nozzle atomizing system.

The master alloy was induction heated at 1200 K in an alumina crucible under a vacuum of 10^{-2} Pa. The melt was teemed through a guide tube, and atomized by a jet of Ar at 4.0 MPa. The $\text{Cu}_{50}\text{Zr}_{40}\text{Ti}_{10}$ powder was collected and sieved in a closed system filled with inert gas. A uniaxial pressing method was conducted with top and bottom stainless steel punches. In order to alleviate the oxidation of the powders, the powders were precompact at pressure between 75 and 225 MPa before hot pressing. The powders were put into a stainless steel mold, heated by a heating buff at a heating rate of 10 K/min, and then hot pressed at pressure between 300 and 600 MPa and temperature between 360 and 400 °C for 30 s. The detailed hot pressing parameters are shown in Table 1. The hot pressed specimens are in a cylindrical shape with a diameter of 10 mm and a height of about 15 mm.

2.3 Testing methods

The amorphous structure of the powder and the compact was examined by X-ray diffractometry (XRD) in reflection with a monochromatic Cu K_{α} radiation. The thermal stability of the amorphous powders was examined by differential scanning calorimetry (DSC) at a heating rate of 0.5 K/s. The density of the specimens was determined by the Archimedeian method. Mechanical properties under uniaxial compression were measured using a mechanical testing machine at a constant crosshead speed which corresponds to the initial strain rate of $5 \times 10^{-2} \text{ s}^{-1}$. The microstructure was characterized by scanning electron microscopy (SEM) and optical microscopy (OM). The experimental results of the compression strength and strain limit are shown in Table 2.

3 Results

3.1 SEM image of gas-atomized powder

The SEM image of the gas-atomized $\text{Cu}_{50}\text{Zr}_{40}\text{Ti}_{10}$ powder is shown in Fig.1. The size of the gas-atomized powder is less than 50 μm . In addition, most of the gas-atomized powders are in spherical form and this can be suitable for the consolidation of powder by hot pressing.

3.2 XRD analysis

The formation of amorphous phase of the gas-atomized $\text{Cu}_{50}\text{Zr}_{40}\text{Ti}_{10}$ powder was confirmed by X-ray diffraction. The XRD pattern of the gas-atomized powder less than 50 μm is shown in Fig. 2. As can be seen in Fig. 2, fully amorphous phase of the gas-atomized powder without any crystallinity is formed in the particle size less than 50 μm . Therefore, the $\text{Cu}_{50}\text{Zr}_{40}\text{Ti}_{10}$ amorphous powders with a particle size less

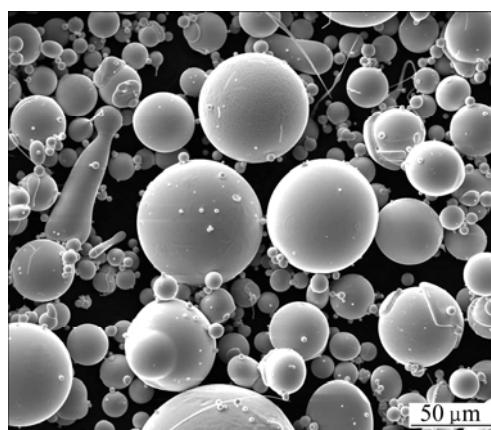


Fig. 1 SEM image of gas-atomized $\text{Cu}_{50}\text{Zr}_{40}\text{Ti}_{10}$ powder

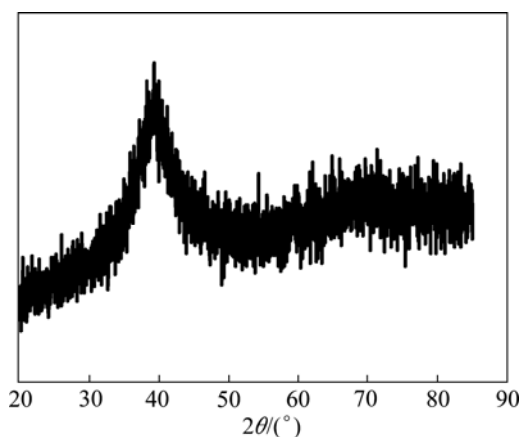


Fig. 2 X-ray diffraction pattern of gas-atomized powder less than 50 μm

than 50 μm were used for subsequent consolidation in this study.

3.3 DSC analysis

The thermal stability and crystallization behavior of the $\text{Cu}_{50}\text{Zr}_{40}\text{Ti}_{10}$ amorphous powders were examined by DSC measurement. Figure 3 shows the DSC curve of the $\text{Cu}_{50}\text{Zr}_{40}\text{Ti}_{10}$ amorphous powder with a particle size less than 50 μm at a constant heating rate of 0.5 K/s. As shown in Fig. 3, the onset temperature of crystallization T_x is 693.2 K. Below the onset of crystallization, the glass transition T_g , which is shown as an endothermic reaction in the DSC curve, occurs at ~ 629.5 K. Thus a fairly large supercooled liquid region ΔT_x of ~ 63.7 K exists in gas-atomized $\text{Cu}_{50}\text{Zr}_{40}\text{Ti}_{10}$ amorphous powder, indicating that the studied amorphous powder can be used to investigate the effect of the consolidation temperature on the properties of the consolidated sample. However, the ΔT_x of the studied amorphous alloy powder is slightly lower than the literature data measured with melt spun $\text{Cu}_{50}\text{Zr}_{40}\text{Ti}_{10}$ amorphous ribbons [23].

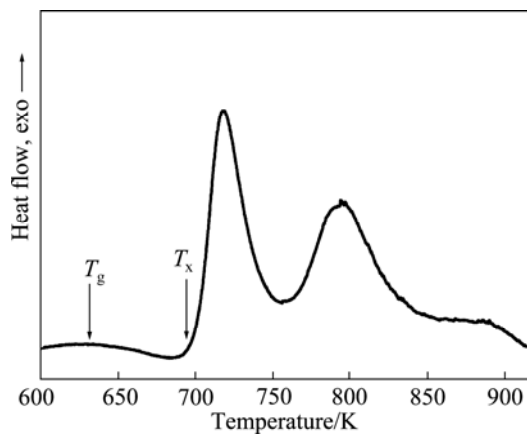


Fig. 3 DSC curve of $\text{Cu}_{50}\text{Zr}_{40}\text{Ti}_{10}$ amorphous powder with particle size less than $50\ \mu\text{m}$ at constant heating rate of $0.5\ \text{K/s}$

3.4 Range and variance analysis

The gas-atomized $\text{Cu}_{50}\text{Zr}_{40}\text{Ti}_{10}$ amorphous powder was consolidated by a hot pressing apparatus without vacuum protection and by degassing procedure, and the bulk amorphous alloy compacts were prepared in the form of cylinder with a diameter of $10\ \text{mm}$ and a height of $\sim 15\ \text{mm}$. The preforming pressure, consolidation pressure and consolidation temperature were varied with parameters on processing the consolidation of amorphous powder. An $L_9(3^4)$ orthogonal test was adopted to investigate the effect of three consolidation parameters on the compression strength and strain limit of the compacts, respectively. The parameters and their corresponding values are shown in Table 1. The compressive stress—strain curves for the compacts are shown in Fig. 4. The measured compression strength and

strain limit of the compacts are listed in Table 2. An analysis of variance of the data was done with the compression strength and strain limit for analyzing the effect of the preforming pressure, consolidation pressure, and consolidation temperature on the total variance of the results, respectively. In order to analyze the significance of three factors on the compression strength and strain limit of the compacts, the fourth column (D) in $L_9(3^4)$ orthogonal array is assigned to the error. Table 3 and Table 4 show the results of the analysis of variance for the strain limit and compression strength, respectively. As shown in Table 3, the deviation of the consolidation temperature (C) is less than that of the error (D). This indicates that the consolidation temperature does not influence the strain limit of the compact, thus the sum of the deviation of C and D is chosen as the deviation of the error. After being done so, it is clearly from Table 3 that

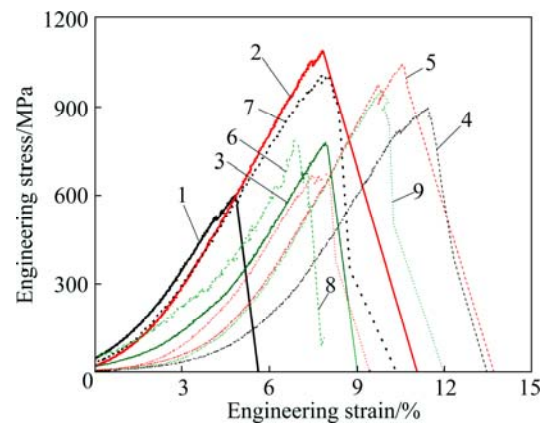


Fig. 4 Compressive stress—strain curves of compacts at strain rate of $5 \times 10^{-2}\ \text{s}^{-1}$ (Numbers 1–9 are test number shown in Table 2)

Table 3 Variance analysis for strain limit

Source of variance	Deviation	Degree of freedom	Variance	F value	Significance	Range	Remark
A	12.51	2	6.26	7.11	Very significant	2.87	
B	13.22	2	6.61	7.51	Very significant	2.90	$F_{0.1}(2,4)=4.32$
C	0.21	2				0.37	$F_{0.05}(2,4)=6.94$
D	3.31	2					$F_{0.01}(2,4)=18.00$
Error	3.52	4	0.88				
Total	29.25	8					

Table 4 Variance analysis for compression strength

Source of variance	Deviation	Degree of freedom	Variance	F value	Significance	Range	Remark
A	12470.58	2				90.34	
B	147555.82	2	73777.91	5.55	Very significant	289.70	$F_{0.1}(2,6)=3.46$
C	19178.20	2				103.54	$F_{0.05}(2,6)=5.14$
D	48068.67	2					$F_{0.01}(2,6)=10.92$
Error	79717.45	6	13286.24				
Total	227273.27	8					

the preforming pressure and consolidation pressure both significantly influence the strain limit of the compact. As shown in Table 4, the deviation of the preforming pressure (A) and consolidation temperature (C) is less than that of the error (D). This indicates that the preforming pressure and consolidation temperature do not influence the compression strength of the compact, so the sum of the deviation of A, C and D is chosen as the deviation of the error. One can find from Table 4 that the consolidation pressure significantly influences the compression strength of the compact.

In addition, the range analysis was also performed on the strain limit and compression strength in order to obtain the optimal consolidation condition for the compacts (see Table 3 and Table 4), respectively. As shown in Table 3, the ascending sequence of the range of three factors for the strain limit is the consolidation temperature, preforming pressure, and consolidation pressure, respectively. As shown in Table 4, the ascending sequence of the range of the factors for the compression strength is the preforming pressure, consolidation temperature, and consolidation pressure, respectively. These results indicate that the influence degree of three factors on the compression strength and strain limit increases according to the ascending sequence of the range, which is also coherent with the results of the analysis of variance.

On the other hand, the averaged values of the strain limit and compression strength for each factor at different levels are plotted in Fig. 5 in order to analyze the relationships between three factors and the mechanical properties, and to obtain the optimal consolidation conditions for the fabrication of the compacts. As shown in Fig. 5, the strain limit and compression strength first both increase and then decrease with the increase of three factors. The strain limit and compression strength both reach up to a maximum at the second level of three factors, respectively. This indicates that the optimum combinations of three factors for the strain limit and compression strength both are $A_2B_2C_2$. Thus the optimum consolidation condition for the $Cu_{50}Zr_{40}Ti_{10}$ amorphous powder is first precompacted under the pressure of 150 MPa, and then consolidated under the pressure of 450 MPa at the temperature of 380 °C, respectively, at the strain limit and compression strength point of view. In addition, the theoretical optimum values for the strain limit and compression strength are both calculated according to the orthogonal theory. The optimal theoretical values are 12.1 % for the strain limit and 1180.7 MPa for the compression strength, respectively, which are slightly higher than the practical optimum values shown in Table 2.

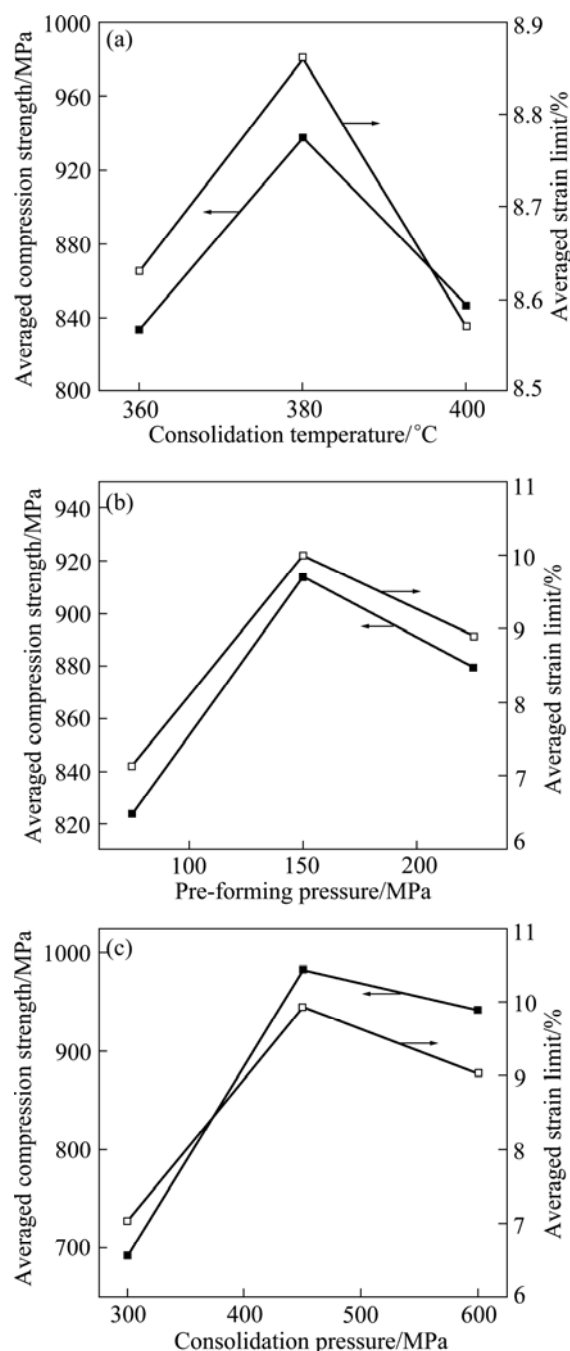


Fig. 5 Averaged values of strain limit and compression strength for each factor at different levels: (a) Consolidation temperature; (b) Preforming pressure; (c) Consolidation pressure

3.5 Microstructure and fractography of compacts

In order to investigate the bonding between the amorphous alloy powders, the polished cross sections of the compacts were examined by using an OM. Figure 6 presents the OM microstructures of the polished cross sections of the compacts consolidated under different consolidation temperatures and consolidation pressures at the preforming pressure of 75 MPa. It is noted that there are the same results for the compacts preformed at other pressures. As shown in Fig. 6, there are many pores

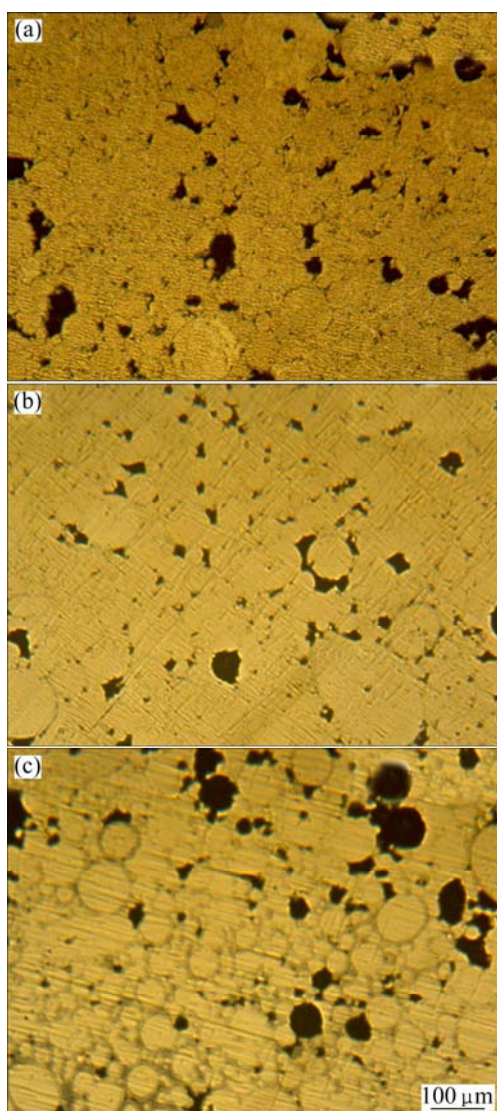


Fig. 6 OM microstructures of polished cross-sections of compacts consolidated under different consolidation temperatures and pressures at preforming pressure of 75 MPa: (a) 300 MPa, 360 °C, $\rho=6.67 \text{ g/cm}^3$; (b) 450 MPa, 380 °C, $\rho=7.03 \text{ g/cm}^3$; (c) 600 MPa, 400 °C, $\rho=6.81 \text{ g/cm}^3$

(dark parts) resulted from the original pores before the consolidation and the pores resulted from the pull-out of the powder during polishing, indicating that the fully densification compact cannot be obtained under the studied conditions. In addition, the density of the compacts first increases with increasing consolidation temperature and pressure and then decreases when the consolidation temperature and the consolidation pressure exceed 380 °C and 450 MPa, respectively. The powder boundary is more and clearer when the consolidation temperature and the consolidation pressure reach up to 380 °C and 450 MPa, respectively.

In addition, SEM imaging was conducted on the fracture surface of the test samples in order to investigate the mechanical response of the compacts. The typical

SEM fractography of the compacts is shown in Fig. 7. The fracture surface shows the classic vein-like and smooth cleavage fracture patterns as well as the fracture along the particle boundaries. In addition, there are many pores between the amorphous alloy powders and the cracks initiate and propagate along the particle boundaries.

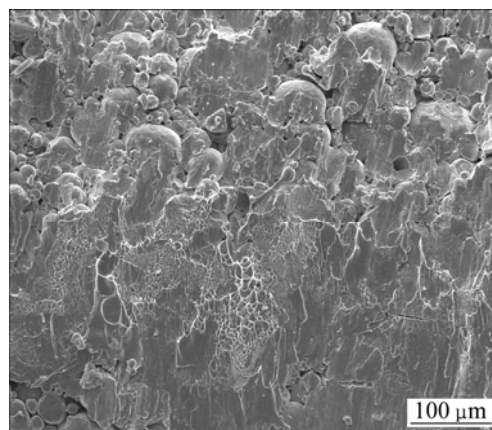


Fig. 7 Typical SEM image of compression specimen fabricated under performing pressure of 75 MPa, consolidation pressure of 450 MPa and consolidation temperature of 380 °C

4 Discussion

It is well known that the mechanical property of the compact depends on the pore, inclusion, amount of particle boundary, and so on. As shown in Fig. 5(a), the compression strength and strain limit of the compacts both first increase with increasing consolidation temperature and then decrease when the consolidation temperature exceeds 380 °C. As indicated in Refs. [25,26], the viscosity of the amorphous alloy decreases with increasing temperature in the supercooled liquid region, thus the deformation capacity of amorphous alloy increases with increasing temperature. It should result in the increase of mechanical property of the compact with increasing consolidation temperature, which is coherent with the results of Ref. [13]. However, the $\text{Cu}_{50}\text{Zr}_{40}\text{Ti}_{10}$ amorphous powders would be oxidized by the residual air in the pores of the precompacts due to without degassing and vacuum protection during heating [27]. Thus the hardness and strength of the amorphous powder are too high to be deformed at ambient temperature even at very high pressure [8,20]. As shown in Fig. 6, the density of the compacts is not improved and the powder boundary is clearer and more when the consolidation temperature reaches up to 400 °C. Thus the effective load area decreases due to the decrease of the density of the compact and the position of the initiation of the cracks increases due to the increase of the magnitude of the powder boundary when the consolidation temperature

reaches up to 400 °C. This indicates that the mechanical property of the compact will decrease when the consolidation temperature reaches up to 400 °C. In order to further clarify this fact, XRD analyses were performed on the compacts consolidated under different consolidation temperatures in Fig. 8. It is clearly seen from Fig. 8 that the compacts are partially oxidized and the oxides are composed of CuO and ZrO₂. The oxidization of the amorphous powder is more and more serious with increasing consolidation temperature. These hard and brittle oxides will deteriorate the consolidation capacity of the powders, but these oxides could play a reinforce role in the compact when the content of these oxides is less than a critical content. The comprehensive effects of two factors would result in the increase of the mechanical properties of the compacts. However, when the content of the oxides increases up to a critical value, the oxides could play not a reinforce role but a deteriorate role. It would result in the decrease of the mechanical properties.

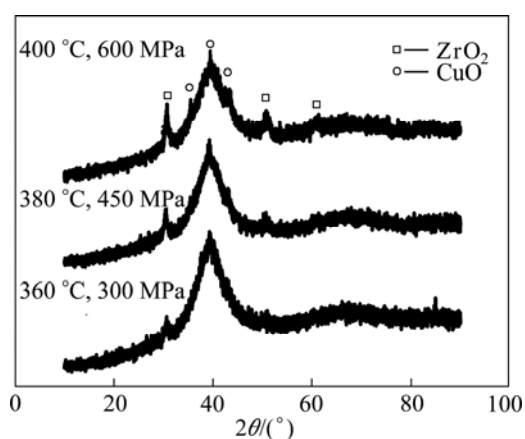


Fig. 8 X-ray diffraction patterns of compacts consolidated at different consolidation temperatures

As shown in Fig. 5(b), the compression strength and strain limit of the compact both increase when the preforming pressure is less than 150 MPa. It would be due to the increase of the densification of the precompact with increasing preforming pressure, resulting in the alleviation of oxidation of the powders. Thus the mechanical properties of the compact are improved. However, the mechanical properties of the compacts decrease when the preforming pressure exceeds 150 MPa. It would be resulted from the formation of the microcracks due to the cracking of the air oxides on the surface of the gas-atomized powder in the precompact under high preforming pressure, resulting in the increase of the air content in the precompact which leads to more serious oxidization of the amorphous powders. Thus the powders are more difficultly consolidated, resulting in

the increase in the defects, inclusions and amount of particle boundaries. In fact, YAN et al [27] investigated the surface structure of Cu-based gas-atomized amorphous powders, and found that amorphous powders were enveloped by a thick (30 nm) oxide ceramic. YAMASAKI et al [28] also found the same phenomenon during investigation of vacuum degassing behavior of Zr-, Ni-, and Cu-based amorphous alloy powders. Therefore, the mechanical properties of the compacts are deteriorated.

As shown in Fig. 5(c), the compression strength and strain limit of the compacts increase with increasing consolidation pressure when the consolidation pressure is less than 450 MPa. It is well known that the densification of the compact increases with increasing consolidation pressure [13], resulting in the increase of the mechanical properties of the compacts. However, the mechanical properties of the compacts decrease when the consolidation pressure exceeds 450 MPa. It would result from not only the formation of the cracks due to the abruption of the oxide film on the surface of the powder but also the increase of the position of the initiation of the cracks due to the increase of the magnitude of the powder boundaries, leading to the decrease of the mechanical properties of the compact under high consolidation pressure. These results are coherent with the results observed from Fig. 6.

As shown in Table 2, the fracture strength of the compact is significantly lower than that of the corresponding amorphous ribbon [23]. The reason would be due to the fact that the structure of the Cu₅₀Zr₄₀Ti₁₀ amorphous ribbon is more homogeneous than that of the compact. As shown in Fig. 6 and Fig. 7, many holes emerge in the compacts, which results in the decrease of the effective load area. At the same time, many powder boundaries can be observed on the polished cross section of the compact in Fig. 6. It is advantageous of the initiation and propagation of the cracks in Fig. 7. These results would lead to the remarkably decrease of the compression strength of the compact. However, the strain limit of the compact is significantly more than that of the Cu₅₀Zr₄₀Ti₁₀ amorphous ribbon [23].

In addition, the compacts exhibit a high strain limit in Fig. 4. As mentioned above, the compact can be considered a porous amorphous/oxide composite. These phenomena are also in agreement with the results of the porous amorphous alloys [29,30] and the amorphous/crystalline composites [31]. The compacts can be largely deformed under low load due to the existence of the holes during initial deformation. With increasing deformation, the sample is gradually densified due to the close of the holes during the compression, and the load area gradually increases. Thus the compacts exhibit the large strain limit.

5 Conclusions

1) The size of the gas-atomized $\text{Cu}_{50}\text{Zr}_{40}\text{Ti}_{10}$ amorphous powders is less than 50 μm . The glass transition temperature (T_g), the crystallization temperature (T_x), and the supercooled liquid region (ΔT_x) of the gas-atomized $\text{Cu}_{50}\text{Zr}_{40}\text{Ti}_{10}$ amorphous powders are 629.5, 693.2, and 63.7 K, respectively.

2) The consolidation pressure significantly influences the strain limit and compression strength of the compact. But the mechanical properties are not significantly influenced by the consolidation temperature. In addition, the preforming pressure significantly influences not the compression strength but the strain limit.

3) The optimum consolidation condition for the $\text{Cu}_{50}\text{Zr}_{40}\text{Ti}_{10}$ amorphous powder is first precompacted under the pressure of 150 MPa, and then consolidated under the pressure of 450 MPa and the temperature of 380 °C.

References

- [1] WANG W H, DONG C, SHEK C H. Bulk metallic glasses [J]. *Mater Sci Eng R*, 2004, 44: 45–89.
- [2] LIU Y H, WANG G, WANG R J, ZHAO D Q, PAN M X, WANG W H. Super plastic bulk metallic glasses at room temperature [J]. *Science*, 2007, 315: 1385–1388.
- [3] INOUE A, HASHIMOTO K. Amorphous and nanocrystalline materials [M]. Heidelberg: Springer, 2001: 1.
- [4] LUBORSKY F E. Amorphous metallic alloys [M]. London: Butterworths, 1983: 506.
- [5] KULKARNI K M. Powder metallurgy for full density products [M]. Princeton: MPIF, 1987: 53.
- [6] LEE P Y, LO C, JANG J S C. Consolidation of mechanically alloyed $\text{Mg}_{49}\text{Y}_{15}\text{Cu}_{36}$ powders by vacuum hot pressing [J]. *J Alloys Compd*, 2007, 434–435: 354–357.
- [7] WEI X, HAN F S, WANG X F, WANG X F, WEN C E. Fabrication of Al-based bulk metallic glass by mechanical alloying and vacuum hot consolidation [J]. *J Alloys Compd*, 2010, 501: 164–167.
- [8] KIM Y B, JANG D H, SEOK H K, KIM K Y. Fabrication of Fe–Si–B based amorphous powder cores by cold pressing and their magnetic properties [J]. *Mater Sci Eng A*, 2007, 449–451: 389–393.
- [9] WEI Xiao-shun, HUANG Yong-jiang, VEKSHIN B S, KRAPOSHIN V S, SHEN Jun. Bulk amorphous $\text{Al}_{85}\text{Ni}_{10}\text{Ce}_5$ composite fabricated by cold hydro-mechanical pressing of partially amorphous powders [J]. *Chinese Science Bulletin*, 2011, 56(36): 3965–3971.
- [10] ZHANG L C, XU J, MA E. Consolidation and properties of ball-milled $\text{Ti}_{50}\text{Cu}_{18}\text{Ni}_{22}\text{Al}_4\text{Sn}_6$ glassy alloy by equal channel angular extrusion [J]. *Mater Sci Eng A*, 2006, 434: 280–288.
- [11] BAE D H, LEE M H, YI S, KIM D H, SORDELET D J. Deformation behavior of a $\text{Ni}_{59}\text{Zr}_{20}\text{Ti}_{16}\text{Si}_2\text{Sn}_3$ metallic glass matrix composite reinforced by copper synthesized by warm extrusion of powders [J]. *J Non-Cryst Solids*, 2004, 337: 15–20.
- [12] KIM H J, LEE J K, SHIN S Y, JEONG H G, KIM D H, BAE J C. Cu-based bulk amorphous alloys prepared by consolidation of amorphous powders in the supercooled liquid region [J]. *Intermetallics*, 2004, 12: 1109–1113.
- [13] KIM C K, LEE S, SHIN S Y, KIM D H. Effects of consolidation temperature and pressure on microstructures and mechanical properties of Cu-based bulk amorphous alloys consolidated by spark plasma sintering [J]. *J Alloys Compd*, 2008, 453: 108–114.
- [14] LI Yuan-yuan, YANG Chao, LI Xiao-qiang, CHEN You. Fabrication of Ti-based composites based on bulk amorphous alloys by spark plasma sintering and crystallization of amorphous phase [J]. *The Chinese Journal of Nonferrous Metals*, 2011, 21(10): 2305–2323. (in Chinese)
- [15] CHEN Wei-ping, WU Xue-mei, YANG Chao, LÜ Ying, QU Sheng-guan, CHEN Min-dan. Bulk $\text{Ti}_{66}\text{Nb}_{18}\text{Cu}_{6.4}\text{Ni}_{6.1}\text{Al}_{3.5}$ fine grain composites reinforced by crystallized phases fabricated by spark plasma sintering [J]. *The Chinese Journal of Nonferrous Metals*, 2011, 21(6): 1285–1291. (in Chinese)
- [16] CHEN Yong, LIANG Jia-hong, YANG Chao, LI Xiao-qiang, XIAO Zhi-yu, LI Yuan-yuan. Fabrication of crystallized $\text{Ti}_{70}\text{Nb}_{7.8}\text{Cu}_{8.4}\text{Ni}_{7.2}\text{Al}_{6.6}$ composites by spark plasma sintering or crystallization of amorphous phase [J]. *The Chinese Journal of Nonferrous Metals*, 2011, 21(6): 1335–1341. (in Chinese)
- [17] SHIN S, SONG M S, KIM T S. Synthesis of diamond-reinforced $\text{Zr}_{65}\text{Al}_{10}\text{Ni}_{10}\text{Cu}_{15}$ metallic glass composites by pulsed current sintering [J]. *Mater Sci Eng A*, 2009, 499: 525–528.
- [18] XIE G Q, LI S, LUZGIN D V L, CAO Z P, YOSHIKAWA N, SATO M, INOUE A. Effect of Sn on microwave-induced heating and sintering of Ni-based metallic glassy alloy powders [J]. *Intermetallics*, 2009, 17: 274–277.
- [19] ANDO S, MINE Y, TAKASHIMA K, ITOH S, TONDA H. Explosive compaction of Nd–Fe–B powder [J]. *J Mater Process Technol*, 1999, 85: 142–147.
- [20] DROZDZ D, LATUCH J, KULIK T. Bulk amorphous cast iron with small boron addition, produced by powder compaction at high pressure [J]. *J Alloys Compd*, 2005, 395: 59–62.
- [21] KIM C K, SON C Y, HA D J, YOON T S, LEE S, KIM N J. Microstructure and mechanical properties of powder-injection-molded products of Cu-based amorphous powders and Fe-based metamorphic powders [J]. *Mater Sci Eng A*, 2008, 476: 69–77.
- [22] INOUE A, ZHANG W, ZHANG T, KUROSAKA K. High-strength Cu-based bulk glassy alloys in Cu–Zr–Ti and Cu–Hf–Ti ternary systems [J]. *Acta Mater*, 2001, 49: 2645–2652.
- [23] AN W K, CAI A H, XIONG X, LIU Y, LUO Y, LI T L, LI X S. Thermal, mechanical and corrosive behaviors of a Cu-based metallic glass [J]. *Adv Mater Res*, 2011, 146–147: 1491–1497.
- [24] CAI A H, AN W K, LI X S, LUO Y, LI T L. Property of Cu–Zr–Ti ternary alloys [J]. *Adv Mater Res*, 2011, 146–147: 1477–1481.
- [25] SCUDINO S, VENKATARAMAN S, STOICA M, SURREDDI K B, PAULY S, DAS J, ECKERT J. Consolidation and mechanical properties of ball milled $\text{Zr}_{50}\text{Cu}_{50}$ glassy ribbons [J]. *J Alloys Compd*, 2009, 483: 227–230.
- [26] LEE J K, KIM H J, KIM T S, KIM Y C, BAE J C. Consolidation behavior of Cu- and Ni-based bulk metallic glass composites [J]. *J Alloys Compd*, 2007, 434–435: 336–339.
- [27] YAN M, YU P, KIM K B, LEE J K, SCHAFFER G B, QIAN M. The surface structure of gas-atomized metallic glass powders [J]. *Scripta Mater*, 2010, 62: 266–269.
- [28] YAMASAKI M, IWAMOTO K, TAMAGAWA H, KAWAMURA Y, LEE J K, KIM H J, BAE J C. Vacuum degassing behavior of Zr-, Ni- and Cu-based metallic glass powders [J]. *Mater Sci Eng A*, 2007, 449–451: 907–910.
- [29] XIE G Q, ZHANG W, LOUZGUINE-LUZGIN D V, KIMURA H, INOUE A. Fabrication of porous Zr–Cu–Al–Ni bulk metallic glass by spark plasma sintering process [J]. *Scripta Mater*, 2006, 55: 687–690.
- [30] WADA T, WANG X M, KIMURA H, INOUE A. Preparation of a Zr-based bulk glassy alloy foam [J]. *Scripta Mater*, 2008, 59: 1071–1074.
- [31] KIM Y B, PARK H M. Synthesis of amorphous/crystalline composite using electroless copper plated amorphous powder [J]. *Mater Sci Eng A*, 2005, 396: 166–171.

固结参数对热压成型铜基块体 非晶合金力学性能的影响

蔡安辉¹, 熊翔², 刘咏², 安伟科¹, 周果君¹, 罗云¹, 李铁林¹, 李小松¹

1. 湖南理工学院 机械工程学院, 岳阳 414006;
2. 中南大学 粉末冶金国家重点实验室, 长沙 410083

摘要: 采用雾化法制备 $\text{Cu}_{50}\text{Zr}_{40}\text{Ti}_{10}$ 非晶合金粉末, 在大气环境下将其热压成型为块体非晶合金, 并基于 $L_9(3^4)$ 正交实验对热压成型条件进行优化。固结成型的 $\text{Cu}_{50}\text{Zr}_{40}\text{Ti}_{10}$ 块体非晶合金的抗压强度和应变极限值分别达到 1090.4 MPa 和 11.9%。固结压力显著影响块体非晶合金的应变极限和抗压强度, 但是固结温度的影响不显著。初始成形力对块体非晶合金的抗压强度的影响不显著而对应变极限的影响很显著。 $\text{Cu}_{50}\text{Zr}_{40}\text{Ti}_{10}$ 非晶合金粉末的最优热压成型工艺条件为: 首先在 150 MPa 压力下进行预成型, 然后在 380 °C 和 450 MPa 条件下进行热压。

关键词: 热压; 铜基非晶合金; 应变极限; 固结; 力学性能

(Edited by LI Xiang-qun)